http://dx.doi.org/10.4314/bajopas.v16i2.2

Bayero Journal of Pure and Applied Sciences, 16(2): 6 - 14
Received: 17/06/2023
Accepted: 04/09/2023
ISSN 2006 – 6996

STRUCTURAL AND DIELECTRIC STUDY OF NANO-CRYSTALLINE $MFe_{12}O_{19}$ (M=Ba and Sr) HEXAFERRITES PREPARED VIA SOL-GEL AUTO-COMBUSTION TECHNIQUES

[1]Musa, I. M., [2]Abdu, Y.[*] and [2]Musa A. O.
[1]Department of Physics, Federal University Dutse, Jigawa State. Nigeria.
[2]Department of Physics, Bayero University, Kano, Nigeria.
[*]Co-author email: ayunusa.phy@buk.edu.ng, yunusa_abdu@yahoo.com
Phone No: 08029174511

ABSTRACT
The structural and electrical properties of m-type hexaferrites are very sensitive to particle size, shape and degree of crystalinity. The syntheses techniques and the nature of cations in the material lead to significant change in electromagnetic properties of the materials. In this work, M-type $BaFe_{12}O_{19}$ and $SrFe_{12}O_{19}$ nanohexaferrites were successfully synthesized via sol-gel auto-combustion techniques. The structural, dielectric and functional group of these nanoparticles was investigated using XRD, FTIR, and Impedance analyzer. The XRD analysis revealed that pure and single phase hexagonal ferrites with crystallites sizes of 33.35nm for $BaFe_{12}O_{19}$ and 32.29nm for $SrFe_{12}O_{19}$ were obtained. The lattice constant slightly varies due to variation of ionic radii in the samples. The FTIR spectra of the sample show three dominants peaks in the range 400-600 cm^{-1} which indicate the formation of the desired hexaferrites structure. The dielectric properties were studied using impedance measurements obtained in the frequency range 100Hz-120MHz. The dielectric constant, dielectric loss and conductivity were analysed using Maxwell-Wagner model. Dielectric constant was enhanced at high frequency in the entire sample and reduction of dielectric loss is also observed with further ions substitutions. The grain boundary resistance contributes the most to the dielectric properties as indicated by Nyquist plot, whereas the Ac conductivity is the dominant conducting mechanism in the material. A high dielectric property, low energy dissipation and higher conductivity were observed with $SrFe_{12}O_{19}$ at higher frequency these make it useful for higher frequency applications.
Keywords: M-type nano-hexaferrites, sol-gel auto-combustion, metal ions substitutions, materials properties.

INTRODUCTION

M-type hexaferrites with SrM ($SrFe_{12}O_{19}$) and BaM ($BaFe_{12}O_{19}$) structure are ferromagnetic material with magnetization along c-axis (Mohammed *et. al.,* 2020). They also possess high resonance frequencies, high resistivity, high saturation magnetization(Ms), high magneto-crystalline anisotropies, Curie temperature(Tc), coercivity(Hc) along with low cost, excellent chemical stability and corrosion resistance low eddy current losses as well as smaller dielectric losses with thermal stability(Maria *et. al.,* 2018, Mukhtar *et. al.,* 2021, Imran *et. al.,* 2011). This makes M-type hexaferrite a viable candidate for various technological applications such as permanent magnets, magnetic recording media ,magneto-optical devices, microwave devices ,etc (Ashraff *et. al.,* 2021, Mohammed *et. al.,* 2021, Tchouank *et. al.,* 2019). The electrical properties of ferrites play vital role in high frequency applications and these are also associated to the dielectrics, the benefits of the ferrites over other dielectrics are their elastic properties, better resistance to environmental alterations, mainly at higher temperature (Shah *et. al.,* 2020). The major factors affecting M-type hexagonal ferrites properties are associated to fabrication techniques and cations distributions (Abdu and Musa, 2021). Several techniques have been employed by various researchers to synthesize M-type hexaferrites. The most extensively used techniques for the bulk preparation of ferrites are the conventional solid-state reactions such as ceramic method, high energy ball milling and flash combustion.

These methods involve milling and firing of the reaction mixture at about 1200^0C or above and thus result in the incorporation of impurities, generation of lattice strain and irregularity in particle shape. Moreover, at high temperature, their particle size tends to be larger due to agglomeration of fine particles (Ashiq *et. al.,* 2017, Mukhtar *et. al.,* 2012, Almesseire *et. al.,* 2019). On the other hand, wet methods do not involve any milling of the starting materials and there is direct mixing of cations on atomic scale. Evolution of gaseous products during exothermic decomposition of the precursor provides heat to the solid-state reaction, thus decreasing the external temperature required, these methods lead to the formation of stoichiometrically pure and single-phase nanosized ferrites with large surface area in shorter time (Abdu and Musa, 2021, Altaf *et. al.,* 2015). Co-precipitation is one of the simplest techniques for the preparation of fine hexaferrite particles. However, such particles strongly agglomerate, so that an additional milling procedure seems to be necessary. A versatile method for preparing submicron particles at low temperature is the sol-gel technique. In addition, recently this method has been found to be a very suitable method for the preparation of multi-component oxide materials at relatively lower temperatures. The major advantages of the method are not only to reduce the product formation temperature but also have good control over its homogeneity, microstructures and decrease in the particle size which results to a high coercivity values that are applicable in high frequency applications (Kajal *et. al.,* 2007, Ibrahim *et. al.,* 2021).

This work presents the synthesis and characterization of pure M-type hexaferrite prepared using sol-gel auto combustion techniques. The work aims to synthesizes pure phase M-type hexaferrites and study the dielectric properties of synthesized M-type hexaferrite. The prepared samples were characterized using XRD, FTIR, and impedance analyzer.

MATERIALS AND SYNTHESIS

Pure M-type hexaferrites with SrM ($SrFe_{12}O_{19}$) and BaM ($BaFe_{12}O_{19}$) structure were synthesized via sol-gel autocombustion technique. The starting materials were obtained from Loba Chemie with 99.9% purity which include $Fe(NO_3)_3.9H_2O$, $Ba(NO_3)_2$, $Sr(NO_3)_2$ and citric acid ($C_6H_8O_7$). The required amounts of the metal salt were weighed in stoichiometric ratios and dissolved in ethylene glycol to form the salt solution, maintaining the molar ratio of citric acid to metal nitrates at 1:1.5. To adjust the pH to 7.00, ammonia solution was added dropwise. The solution was then heated with a magnetic heating stirrer at 80-100 ^{o}C for 3 hours which evaporated the ethylene glycol and obtained the viscous gel solution. The solution was then heated at 280-300 ^{o}C for about 30 minutes which resulted in autocombustion thereby turning the gel into fluffy precursor powder. This process was accompanied by emission of volatile gases of HNCO, NH_3, and N_2. The precursor materials were calcinated at 1100 ^{o}C for 6 hours to obtain the desired hexagonal phase.

Sample Characterization

The characterization of the synthesized samples was done using X-ray Diffraction Machine (XRD), Impedance analyser, Field emission Scanning Electron Microscopy (FESEM), Energy Dispersive X-ray Spectroscopy

RESULTS AND DISCUSSION

The structural, functional group and impedance analysis was carried out, presented and discussed. The discussion is based on the XRD, Fourier transform (FTIR) and Impedance analyzer spectra obtained for the synthesized hexaferrite samples. Other computations carried out on the samples have also been presented and discussed.

XRD Analysis

The x-ray diffractometer (XRD) (Bruker AXSD8 advance diffractometer) was used to study the structure of the synthesized M-type hexaferrites. XRD patterns were recorded between 20°–80° range.

The XRD spectra of $BaFe_{12}O_{19}$ and $SrFe_{12}O_{19}$ are shown in Fig. 1. The diffraction peaks were indexed using JCPDS card no. 39–1433. The XRD peaks show the occurrence of pure M-type magnetoplumbhite hexagonal structure without impurities. The values of the lattice parameters were calculated and presented in Table 1. There is slight variation in values of the lattice parameters of $BaFe_{12}O_{19}$ and $SrFe_{12}O_{19}$ this arises as a result of variation in ionic radii of Ba^{2+} (1.35 Å) and Sr^{2+} (1.12 Å). The c/a ratio of all the samples is not greater than 3.98 as shown in table 1, this implies that all the samples exhibits hexagonal structure, due to the fact that hexaferrite materials can be regarded as having hexagonal structure when c/a ratio of the material is not greater than 3.98 (Ibrahim *et. al.,* 2021). The values of the crystallites size obtained are 33.35nm for $BaFe_{12}O_{19}$ and 32.29nm for$SrFe_{12}O_{19}$, as

presented in Table 2. The crystallite size varies due to variation of ionic radii with Ba^{2+} (1.35 Å) and Sr^{2+} (1.12 Å).The strain(η) observed in the sample occurred during synthesis and calcination processes. The variation of the strain(η) may be attributed to improvement towards pure hexagonal structure(Abdu and Musa, 2021, Ibrahim *et. al.,* 2021).

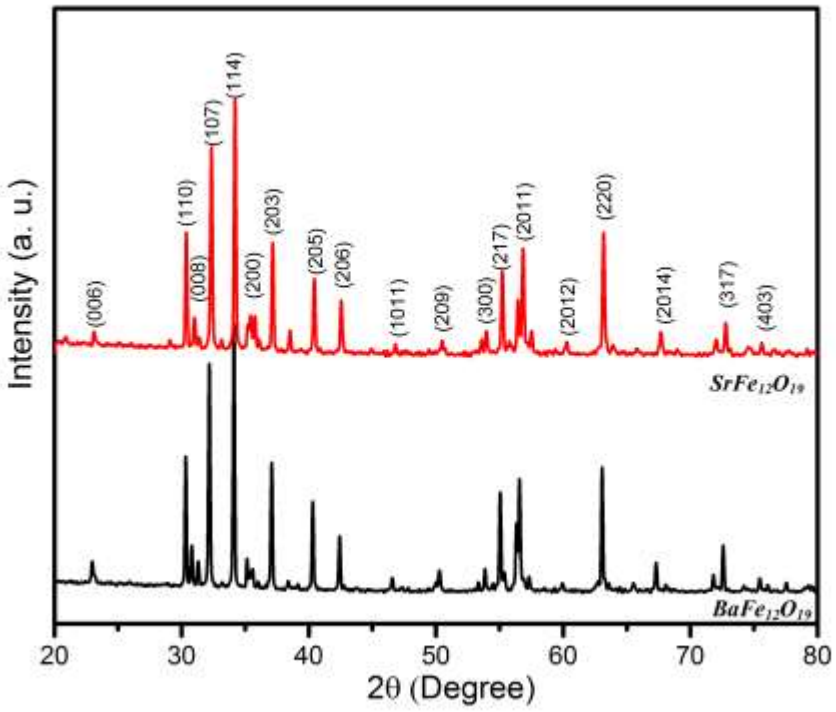

Figure 1 XRD spectra of $BaFe_{12}O_{19}$ .and $SrFe_{12}O_{19}$

Table 1. Calculated Structural parameters from XRD result

Sample	2θ(Degree)	d(Å)	β(Degree)	a(Å)	c(Å)	V(Å^3)	c/a	D(Å)	η	ε
$BaFe_{12}O_{19}$	30.285	2.949	0.244	5.898	23.280	701.728	3.947	333.540	-0.00376	0.00057
$SrFe_{12}O_{19}$	30.243	2.953	0.252	5.906	23.250	702.695	3.937	322.920	-0.00389	0.00059

FTIR Analysis

Fourier transform infrared (FTIR) spectrometer (Nicolet FTIR interferometer IR prestige-21(model-8400S)) was used to study the nature of the attached functional groups of the material. The room temperature FTIR spectra were recorded in the wavenumber range 4000cm-^{1} and 400cm-^{1}.

The FTIR spectra $BaFe_{12}O_{19}$ and $SrFe_{12}O_{19}$is shown in Figure 2. The characteristics bands were observed on each spectrum between 400-600 cm^{-1}range, specifically at 578 cm^{-1},543 cm^{-1} and 421cm^{-1}. These prominent peaks correspond to a symmetric stretching and out plane vibrations of metal oxide (Fe-O) in octahedral and tetrahedral sites and give an idea of the formation of hexaferrites (Abdu and Musa, 2021, Ibrahim *et. al.,* 2021). The observed peak at 898 cm^{-1} is related to O-Fe-O vibration mode. The small band around 1462 cm^{-1} reveals the vibration of metal oxygen metal (M-O-M) bond, which is represented by iron-oxygen-iron. The less intense fascinating bands around 2061cm^{-1} and 2360 cm^{-1} could be assigned to the O-C-O stretching bands. The peak at 3405 cm^{-1} corresponds to the vibration of the hydroxyl group in the sample which is attributed to bending mode of H-O-H.

Dielectric and Impedance Spectroscopy

The room temperature impedance spectra was recorded with impedance analyzer (Wayne Kerr 6500B) having 0 to +40V DC bias voltage and 0 to 100mA DC bias Current in 100Hz to 120MHz frequency range. This was used to calculate the dielectric parameters such as dielectric constant, dielectric loss and AC conductivity. However, prior to the impedance measurement, 9mm thickness pellets were prepared and coated with silver conducting paint to make them suitable for use in the measuring instrument.

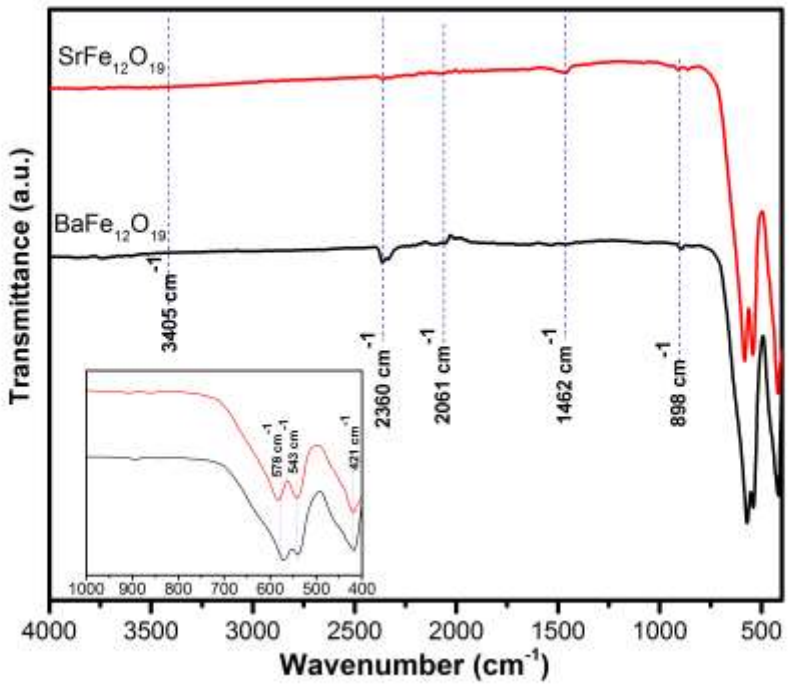

Figure 2 FTIR spectra of $BaFe_{12}O_{19}$ .and $SrFe_{12}O_{19}$

Fig. 3a and 3b shows the variation of ε′ (dielectric constant) and ε′′ (dielectric loss factor) as a function of frequency for $BaFe_{12}O_{19}$ and $SrFe_{12}O_{19}$. It was observed that the ε′ (dielectric constant) and ε′′ (dielectric loss) decreases sharply with the rise in frequency at lower frequency up to intermediate frequency, and slightly rises at higher frequency in $SrFe_{12}O_{19}$. However, $BaFe_{12}O_{19}$show the same behavior with lower and intermediate frequency, whereas in higher frequency region it becomes almost independent of frequency. The high value observed at lower frequencies could be attributed to the presence of oxygen vacancies, interfacial dislocation, grain boundary defects, and the occurrence of large number of electrons hopping between Fe^{3+} and Fe^{2+}(Abdu and Musa, 2021, Mohammed *et. al.,* 2021). Moreover, the slight increase in ε' at higher frequencies, will reduces the penetration depth of EM waves by increasing the skin effect (Mohammed *et. al.,* 2021, Ibrahim *et. al.,* 2021). It can also be observed that $SrFe_{12}O_{19}$has higher dielectric properties compared$BaFe_{12}O_{19}$.

Figure 4 present the variation of dielectric loss factor/ tan δ as a function of frequency for $BaFe_{12}O_{19}$ and $SrFe_{12}O_{19}$. Similar to the trend observed for ε′ with frequency, the tanδ values decreases with the increase in frequency at lower and intermediate frequency, and increases at higher frequencies. These variations seen with tanδ against the frequency can be ascribed to the phenomenon of conduction in ferrites, similar to the Koop's phenomenological theory [6-7]. Lagging of polarization behind ac field dielectric loss arises and may be initiated by the impurities present, grain boundaries and crystal lattice imperfections [13].

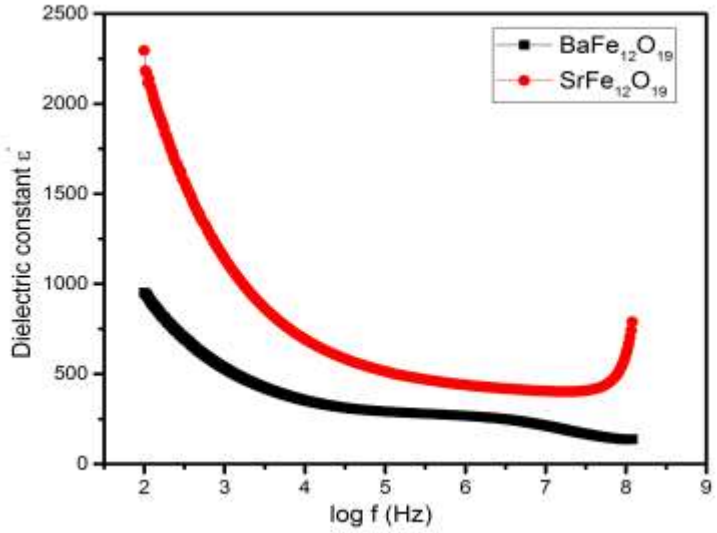

Fig. 3a shows the variation of ε′ as a function of frequency for $BaFe_{12}O_{19}$ and $SrFe_{12}O_{19}$

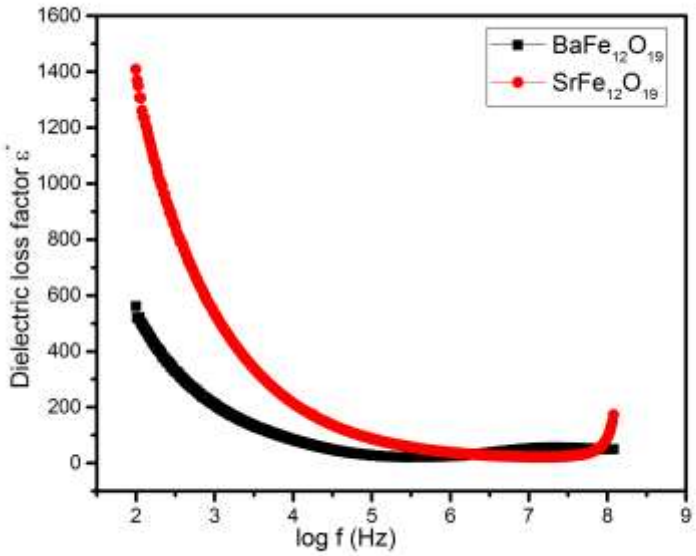

Fig. 3b shows the variation of ε′′ as a function of frequency for $BaFe_{12}O_{19}$ and $SrFe_{12}O_{19}$

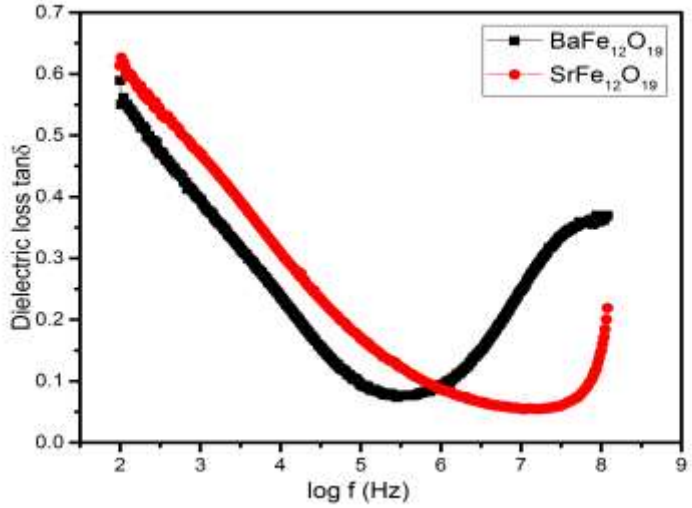

Figure 4 the variation of tan δ as a function of frequency for $BaFe_{12}O_{19}$ and $SrFe_{12}O_{19}$.

It was reported from various researchers that; a polycrystalline hexagonal ferrite sample is consist of grains (or parallel conducting plates) separated by grain boundaries (or resistive plates) (Mohammed *et. al.,* 2019*,* Ibrahim *et. al.,* 2021). These resistances contribute the dielectric and conducting behavior of the ferrite's material. In order to understand the nature and contributions of the grain and grain boundary resistance of the synthesized samples a Nyquist/cole-cole plots was used. This is a plot of the imaginary part (Z'') versus real part (Z') of complex impedance (Z^*) which consists of a semi-circle arc starting from the lower frequencies side to the higher frequencies side. The part of the semi-circle at the lower frequency side represents contribution of the grain boundaries (or grain boundary resistance (R_{gb}) while the part of the semi-circle at the higher frequency side of the Cole-Cole plot represents contribution from the grains (or grain resistance (R_g) (Abdu and Musa, 2021). Figure 5 presents the Cole-Cole plot of $BaFe_{12}O_{19}$ and $SrFe_{12}O_{19}$. It was observed that there is no higher frequency arc for all the substituted samples. Hence, we can conclude that there is no or less contribution from R_g towards the dielectric properties for these samples.

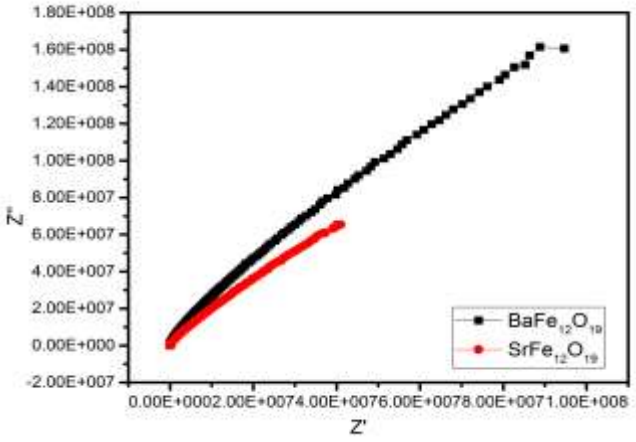

Figure 5: The Cole-Cole plot of $BaFe_{12}O_{19}$ and $SrFe_{12}O_{19}$

Figure 6 show the change of ac conductivity with frequency of $BaFe_{12}O_{19}$ and $SrFe_{12}O_{19}$hexaferrite. It was observed from figure 6 that, the AC conductivity exhibits frequency independent behavior from lower to intermediate frequencies, but a sudden and abrupt rise in σ_{ac} of the prepared samples was observed in all the samples at higher frequency. This behavior is attributed to the fact that, at lower frequencies grain boundaries are more

vigorous; therefore, the hopping frequency of electron among ferric (Fe^{3+}) and ferrous (Fe^{2+}) ion is small at lower frequencies(Mohammed *et. al.,* 2021*,* Ibrahim *et. al.,*2021,). The conductive grains turn out to be more active as the frequency of applied field increases, thereby encouraging carriers hopping among two neighboring octahedral sites and a conversion between ferrous (Fe^{2+}) and ferric (Fe^{3+}) ions (Mohammed *et. al.,* 2019*,* Ibrahim *et. al.,* 2021, Abdu and Musa,2021). Thus, conductivity linearly rises with frequency. Moreover, dispersion at high frequency is due to the conductivity of grains.

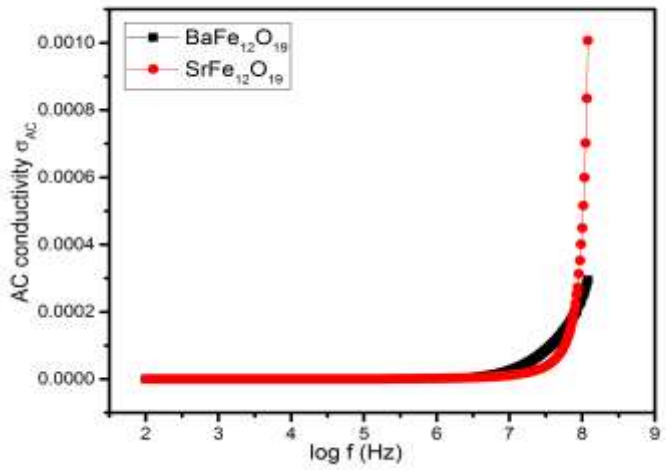

Fig. 6 the variation of ac conductivity with frequency of $BaFe_{12}O_{19}$ and $SrFe_{12}O_{19}$

The variation of $ln\sigma_{ac}$ with $ln\omega$ for $BaFe_{12}O_{19}$ and $SrFe_{12}O_{19}$ is presented in fig. 7. A linear relationship was observed between $ln\sigma_{ac}$ and $ln\omega$ with $ln\sigma_{ac}$ increasing steadily with increase in $ln\omega$, the slope of this linear graph gives the value of the exponent "s" in eqn. (1.0). It has been reported that the value of "s" usually lies between 0 and 1 and that when s = 0, the conduction mechanism is independent of frequency (i. e. DC conductivity) whereas it is dependent on frequency (i. e. AC conductivity) when s ≤ 1[13]. The slope of the linear plot of our sample (Fig. 7) was found to be approximately 1.0 for both the samples. Hence, we can conclude AC conductivity to be the dominant conduction mechanism in the samples.

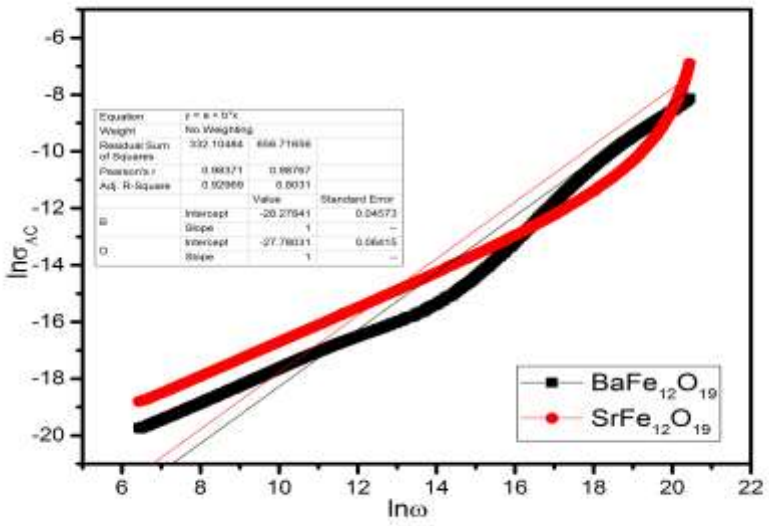

Fig. 7 The variation of $ln\sigma_{ac}$ with $ln\omega$ for $BaFe_{12}O_{19}$ and $SrFe_{12}O_{19}$

Table 2; calculate electrical parameters from Nova1.11

SAMPLE CODE	R_g	C_g	R_{gb}	C_{gb}	σ_{AC}
$BaFe_{12}O_{19}$	-2.89E+06Ω	9.98pF	1.89E+04Ω	5.94pF	2.95E-04
$SrFe_{12}O_{19}$	-4.49E+05Ω	8.22pF	5.41E+04Ω	7.39pF	1.01E-03

CONCLUSION

M-type $BaFe_{12}O_{19}$ and $SrFe_{12}O_{19}$ nanohexaferrites were successfully synthesized via solgel autocombustion techniques. The formation of pure single phase hexagonal ferrites was confirmed from XRD analysis, the crystallites sizes are 33.35nm for $BaFe_{12}O_{19}$ and 32.29nm for $SrFe_{12}O_{19}$was obtained. The crystallite size varies due to variation of ionic radii with Ba^{2+} (1.35 Å) and Sr^{2+} (1.12 Å). the lattice constants slightly varies due to variation of ionic radii in the samples. The FTIR spectra of the sample show three dominants peaks in the range 400-600 cm^{-1} which indicate the formation of the desired hexaferrites structure. The dielectric properties were studied using impedance measurements obtained in the frequency range 100Hz-120MHz. The dielectric constant, dielectric loss and conductivity were analysed using Maxwell-Wagner model. Dielectric constant was enhanced at high frequency in the entire sample and reduction of dielectric loss is also observed with further ions substitutions. The grain boundary resistance contributes the most to the dielectric properties as indicated by Nyquist plot, whereas the Ac conductivity is the dominant conducting mechanism in the material. A high dielectric property, low energy dissipation and higher conductivity were observed with $SrFe_{12}O_{19}$ at higher frequency these makes it useful for higher frequency applications.

REFERENCES

Abdu Y. and Musa I. M. (2021). Structural and Dielecrtic Study of Sr^{2+} barium hexaferrites. Transaction of the Nigerian association of mathematical physics vol 14(January-march issue), 2021, 187-194

Abdu Y. and Musa I. M. (2021) Effect of Al^{+3}, Pr^{+3} and Mn^{+2} substitution on the Structural and Dielecrtic properties of M-type barium hexaferrites. JOSMED vol 17(1), march, 2021, 1-13

Almesseire, M.; Unal, B.; Baykal, A. (2019) Electrical Properties of Cerium and Yttrium co-substituted Strontium nanohexaferrites. J. Inorg. Organomet. Polym. Mater. **2019**, 29, 402–415.

Altaf, F.; Atiq, S.; Riaz, S.; Naseem, S. (2015) Synthesis of Co-doped Sr-hexaferrites by Sol-gel Auto-combustion and its Electrical Characterization. Mater. Today Proc. **2015**, 2, 5548–5551.

Maria Yousaf Lodhi, Muhammad Azhar Khan, Majid Niaz Akhtar,Muhammad Farooq Warsi, Asif Mahmood, Shahid M. Ramay (2018) Role of Nd-Ni on structural, spectral and dielectric properties of strontiumbarium based nano-sized X-type ferrites Ceramics International 44 (2018) 2968–2975

Ashiq, M.N.; Asi, A.S.; Farooq, S.; Haq, M.N.; Rehman, S. (2017) Magnetic and electrical properties of M-typenano-strontium hexaferrite prepared by sol-gel combustion method. J. Magn. Magn. Mater. **2017**, 444,426–431.

Ashraff K.S., Ali, M.M. Ravikumar, J. Mohammed, Naeim Farouk, V. Mohanavel, M. Ravichandran. (2021) Investigation of Ku band microwave absorption of three-layer BaFe12O19, carbon-fiber@Fe3O4, and graphene@BaFe12O19@Fe3O4 composite. Journal of Alloys and Compounds 884 (2021) 161045

Mohammed J., Khalid Mujasam Batoo, A.S. Abdulaziz, A.S. Safana, H.Y. Hafeez, Emad H. Raslan, Muhammad Hadi, AbdulAziz K. Assiafan, Ahamad Imran, A. K. Srivastava(2021). Crystal structure refinement and the magnetic and electro-optical properties of Er3+–Mn2+-substituted Y-type barium hexaferrites. Ceramics International 47 (2021) 18455–18465

Mohammed J., Jyoti Sharma, K.U. Yerima, T. Tchouank Tekou Carol, D. Basandrai, Arun Kumar, Pradip K. Maji, A.K. Srivastava(2020) Magnetic, M€ossbauer and Raman spectroscopy of nanocrystalline Dy3+-Cr3+ substituted barium hexagonal ferrites Physica B 585 (2020) 412115

Mohammed, J., Hafeez, H. Y., Carol, T. T. T., Sharma, J., Isma'il, U. T., Godara, S. K., & Srivastava, A. K. (2019). Structural, dielectric and magnetic properties of Al-

Mn substituted nano-sized M-type strontium hexagonal ferrites. Materials TodayProceedings, 18, 533-541. doi:10.1016/j.matpr.2019.06.392

Mohammed, J., Tchouank Tekou Carol T., Basandrai, D., Gopala R., Bhadu, S., Kumar, Narang, S. B., Srivastava A. K.(2019) "Design of nano-sized ¬ Pr3+–Co2+ substituted M-type strontium hexaferrites for optical sensing and electromagnetic interference (EMI) shielding in ¬ K u band," Appl. Phys. A, 125, 251 https://doi.org/10.1007/s00339-019-2545-5

Mukhtar Ahmad, R. Grössinger, M. Kriegisch, F. Kubel , M.U. Rana (2012) Magnetic and microwave attenuation behavior of Al-substituted Co2W hexaferrites synthesized by sol-gel autocombustion process. Current Applied Physics 12 (2012) 1413e1420

Mukhtar G., Mohammed J., Tchouank Tekou Carol T., N. Halilu, Shaweta Sharma, U. M. Isah, Sachin Kumar Godara, A.K. Srivastava (2021) Investigation of crystal structure, dielectric response and magnetic properties of Tb3+ substituted Co2 Y-type barium hexaferrites Solid State Sciences 113 (2021) 106549

Ibrahim Murtala Musa, Yunusa Abdu, Jibrin Mohammed, and Ajeet Kumar Srivastava (2021). Structural, Dielectric and Raman Spectroscopy of La^{3+}–Ni^{2+}–Zn^{2+} Substituted M-Type Strontium Hexaferrites. *Cryst. Res. Technol.* **2021**, 2100005 **DOI: 10.1002/crat.202100005**

Imran Khan, Imran Sadiq, Muhammad Naeem Ashiq, Mazhar-Ud-Din Rana (2011) Role of Ce–Mn substitution on structural, electrical and magnetic properties of W-type strontium hexaferrites Journal of Alloys and Compounds 509 8042– 8046

Kajal K. Mallick , Philip Shepherd, Roger J. Green (2007) Dielectric properties of M-type barium hexaferriteprepared by co-precipitation Journal of the European Ceramic Society 27 2045–2052

Shah S., O. P. Pandey, J. Mohammed, A. K. Srivastava, A. Gupta, D. Basandrai S. Shah, O. P. Pandey , J. Mohammed, A. K. Srivastava, A. Gupta, D. Basandrai (2020)Reduced graphene oxide (RGO) induced modification of optical and magnetic properties of M-type nickel doped barium hexaferrite Journal of Sol-Gel Science and Technology January 2020 https://doi.org/10.1007/s10971-019-05210-0

Tchouank Tekou Carol Trudel, Jibrin Mohammed, Hafeez Yusuf Hafeez, Bilal Hamid Bhat, Sachin Kumar Godara, and Ajeet Kumar Srivastava (2019) Structural, Dielectric, and Magneto-Optical Properties of Al-Cr Substituted M-Type Barium Hexaferrite J. Phys. Status Solidi A 2019, 1800928